20th Australasian Fluid Mechanics Conference
Perth, Australia
5-8 December 2016

Wall modeling in complex geometry and application to large-eddy simulation of turbulent flow over an airfoil

Wei Gao[1], **Wei Zhang**[1] **and Ravi Samtaney**[1]

[1]Mechanical Engineering, Division of Physical Sciences and Engineering
King Abdullah University of Science and Technology (KAUST), Thuwal 23955-6900, KSA

Abstract

Resolving the energy-containing eddies near the wall in high Reynolds number wall-bounded turbulent flows requires grid sizes of order $O(Re^{13/7})$. Wall-modeled large-eddy simulation (WMLES) leads to a relaxation of this resolution constraint. The proposed wall model predicts the the velocity components on a "virtual wall" located at some distance above the solid wall rather than resolving the near-wall region. The wall-modeling approach appears to a tenable solution for LES of high-*Re* wall-bounded turbulent flows. In this work, we develop a generalized wall model for complex geometry of relevance to engineering applications such as aircraft and wind turbines. The virtual wall model, originally developed by Chung & Pullin (J. Fluid Mech., 2009), is extended to the curvilinear coordinates and implemented for a body-fitted structured mesh. This model dynamically couples the outer resolved region with the wall region, and offers a slip velocity boundary condition for the filtered velocity field on the virtual wall. The wall-model is verified by comparing our WMLES results of NACA airfoil cases at different *Re* against direct numerical simulation. Numerical results indicate that the current model is effective in predicting separation.

Introduction

The main obstacle to the application of large-eddy simulations (LES) to wall-bounded flows is the CPU time required to resolve all the integral scales of motion [1]. The near-wall eddies scale with wall units, and this feature of wall-bounded turbulent flows induces a significant computational cost to sufficiently resolve them in simulations. The resolution problem is exacerbated at high Reynolds number (*Re*) turbulent flows. Choi & Moin [2] estimated that the number of mesh points for wall-resolved large-eddy simulations (WRLES) is $O(Re^{13/7})$, while for wall-modeled large-eddy simulations (WMLES), the mesh point requirements scale linearly with increasingly Reynolds number, i.e., $N_{wm} \sim O(Re)$, where N_{wm} is the number of mesh points needed in WMLES. Hence, the wall modeling approach is a tenable solution for LES of high *Re* wall-bounded turbulent flows.

In the past four decades, several wall models have been proposed for flow in simple geometries, such as channel and flat plate boundary layer flows. However, there are a couple of primary challenges when it comes to practical engineering simulations. First, most wall models follow the equilibrium stress assumption and imply a log-law profile in the near-wall region, which break down when turbulent boundary layers are subjected to strong adverse pressure gradients leading to separation, extra strains due to curvature etc. [1]. Second, most wall modeling strategies fall into the hybrid RANS/LES methods in complex geometries, which solves the RANS equations in an inner layer and provides wall shear stress boundary conditions for the outer LES region [3]. This hybrid method is not only sensitive to the choice of the RANS model and its associated model coefficients, but also cause the so-called "scale disparity" problem on the nominal interfaces between the RANS and LES regions.

Chung & Pullin (2009) [4] proposed the virtual wall model, which dynamically couples the outer resolved region with the wall region, and offers a slip velocity boundary condition for the filtered velocity field on the "virtual" wall. This wall model achieves success in canonical flows without separation [5, 6], and then extended by Cheng *et al.* (2015) [7] to simulate the flat plate turbulent boundary layer flows with separation and reattachment. In the present paper, the virtual wall model is extended to the generalized curvilinear coordinates, and implemented in the structured mesh environment to simulate the flow past different airfoils.

The main goal of our current research is to develop the WMLES code to simulate turbulent flows in complex geometries. In the present paper, we present WMLES results for two airfoil cases, viz., NACA0012 and NACA4412 at $Re = 10^4$ and $Re = 4 \times 10^5$. The paper is organized as follows: we first present the governing equations, the subgrid-scale (SGS) model and the solution method followed by details of the wall model. Finally, some numerical results for the airfoil flows are analyzed and discussed.

Numerical Details

The filtered incompressible Navier-Stokes equations in the generalized curvilinear coordinates are

$$\frac{\partial U^m}{\partial \xi^m} = 0, \tag{1}$$

$$\frac{\partial \left(\sqrt{g} v_i\right)}{\partial t} + \frac{\partial F^{im}}{\partial \xi^m} = 0, \tag{2}$$

where $\xi^m (m = 1,2,3)$ denotes generalized curvilinear coordinates; and U^m and F^{im} are given by

$$\begin{aligned} U^m &= \sqrt{g} v_j \frac{\partial \xi^m}{\partial x_j} = \sqrt{g} u^m, \\ F^{im} &= U^m v_i + \sqrt{g} p \frac{\partial \xi^m}{\partial x_i} - \frac{1}{Re} G^{mn} \frac{\partial v_i}{\partial \xi^n} + \sqrt{g} \frac{\partial \xi^m}{\partial x_j} T_{ij}, \\ \sqrt{g} &= J^{-1} = \det\left[\frac{\partial x_i}{\partial \xi^j}\right], \; G^{mn} = \sqrt{g} \frac{\partial \xi^m}{\partial x_r} \frac{\partial \xi^n}{\partial x_r}, \end{aligned} \tag{3}$$

where $x_j (j = 1,2,3)$ denotes Cartesian coordinates (note that the spanwise direction $x_3 \equiv z$ is aligned with ξ^3). p is the pressure, v_j is the velocity in the Cartesian system, u^m is the contravariant velocity in the generalized curvilinear coordinates, U^m is the volume flux normal to the surface of constant ξ^m, G^{mn} is the mesh skewness tensor. T_{ij} is the subgride-scale (SGS) stress tensor modeled by the stretched-spiral vortex model originally developed by Misra and Pullin [8].

The governing equations are discretized as

$$\frac{\delta U^m}{\delta \xi^m} = 0,$$

$$\sqrt{g}\frac{v_i^{n+1}-v_i^n}{\Delta t} = \frac{3}{2}\left(C_i^n + S_i^n\right) - \frac{1}{2}\left(C_i^{n-1} + S_i^{n-1}\right) + R_i(p^{n+1}) + D_i(v^{n+1}), \quad (4)$$

where $\delta/\delta\xi_m$ represents the energy conservative fourth-order finite difference operator [9], C_i and S_i represent the convective terms and SGS terms, D_i and R_i are discrete operators for the viscous term and the pressure gradient term, respectively. These quantities are

$$C_i = -\frac{\delta}{\delta\xi^m}(U^m v_i),\ S_i = -\frac{\delta}{\delta\xi^m}\left(\sqrt{g}\frac{\delta\xi^m}{\delta x_j}T_{ij}\right),$$
$$R_i = -\frac{\delta}{\delta\xi^m}\left(\sqrt{g}\frac{\delta\xi^m}{\delta x_i}\right),\ D_i = \frac{\delta}{\delta\xi^m}\left(\frac{1}{Re}G^{mn}\frac{\delta}{\delta\xi^n}\right). \quad (5)$$

The fractional step method [10, 11] is used to solve the governing equations. This method follows the predictor-corrector procedure, and the pressure Poisson equation is solved using the multigrid method with line-relaxed Gauss-Seidel as a smoother. The codes have been parallelized using standard MPI-protocol. To achieve near-optimal load balancing, the mesh is divided into blocks of equal size and each of them is assigned to a unique processor. The simulations are performed on the Shaheen-Cray XC40 at KAUST.

Wall Model and Boundary Conditions

In the $\xi - z$ plane, we define the magnitude of the resultant velocity (q) as illustrated in Figure 1. The surface streamlines and the angle θ are essentially determined by the velocity field at the first grid point above the virtual wall. The virtual wall is lifted above the solid wall with some constant height (h_0), and the wall model offers boundary conditions for the outer LES region rather than resolving the near-wall region [4].

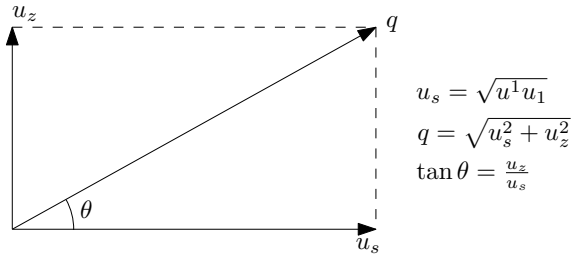

Figure 1: Sketch of the velocity at the virtual wall, u_s and u_z are the streamwise and spanwise velocity components respectively.

Following the idea of near-wall filtering and inner scaling assumption [4], we extended this wall model to curvilinear coordinates. The governing equation for the wall shear stress (τ_w, similar to [7]) and Dirichlet boundary conditions for the velocity at the virtual wall are as follows:

$$q|_{h_0} = \begin{cases} \begin{cases} u_\tau\left(\frac{1}{\mathscr{K}_1}\log\left(\frac{h_0^+}{h_\nu^+}\right) + h_\nu^+\right), & h_0^+ > h_\nu^+, \\ u_\tau h_0^+, & h_0^+ < h_\nu^+, \end{cases} & \tau_{w,\xi} > 0, \\ u_\tau h_0^+, & \tau_{w,\xi} \le 0, \end{cases}$$

where $q|_{h_0}$ is the resultant velocity at the virtual wall, $\tau_w = \mu\frac{\partial q}{\partial\eta}\Big|_0$, $\tau_{w,\xi}$ ($= \tau_w\cos\theta$) is the streamwise wall shear stress, u_τ ($= \sqrt{\tau_w/\rho}$) is the friction velocity, $\mathscr{K}_1$ is the Kármán-like constant, $h_0^+ = h_0 u_\tau/\nu$, $h_\nu^+ = 11$.

For the boundary conditions, we impose a uniform flow $(u,v,w) = (1,0,0)$ at the inlet, convective boundary condition on the outflow plane and periodic boundary condition in the spanwise direction.

Results and Discussions

The physical set-up and domain size are illustrated in Figure 2. It should be noted that a sufficiently long spanwise domain size (L_z) is important for the proper development 3D turbulent structures, and here we use $L_z = 0.8C$, where C is the chord length, as recommended by Zhang & Samtaney (2016) [12] in their direct numerical simulations of flow past an airfoil.

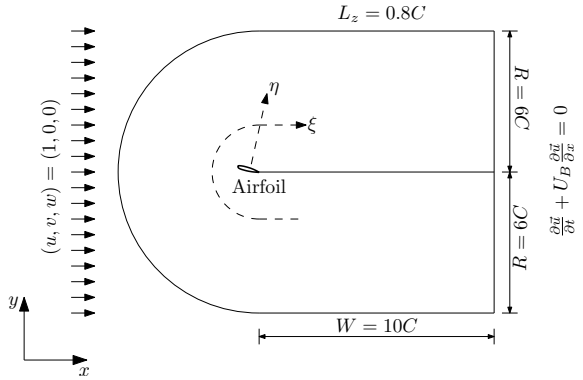

Figure 2: Sketch of the computational domain.

We performed simulations for two different airfoil cases: NACA0012 (symmetric) and NACA4412 (asymmetric). The NACA0012 case at low Reynolds number ($Re = 10^4$) is explored using both direct numerical simulation (DNS) and wall-modeled large-eddy simulation (WMLES). For the NACA4412 case at high Reynolds number ($Re = 4\times10^5$) we perform WMLES with similar geometric parameters as the DNS results recently presented by Hosseini *et al.* (2016) [13]. Simulation parameters for all cases are listed in Table 1.

NACA0012				
Case	*AoA*	*Re*	Mesh	Total time
DNS	5°	10^4	$2048\times256\times128$	$36C/U_0$
WMLES	5°	10^4	$1024\times128\times64$	$50C/U_0$
NACA4412				
Case	*AoA*	*Re*	Mesh	total time
WMLES	5°	4×10^5	$2048\times256\times128$	$5C/U_0$

Table 1: Summary of the numerical simulations. DNS denotes "direct numerical simulation", WMLES denotes "wall-modeled large-eddy simulation", *AoA* is the angle of attack of the airfoil. C/U_0 is the convective time, where U_0 is the inflow velocity and C is the airfoil chord length.

NACA0012 Case: The time- and spanwise-averaged results for NACA0012 (pressure coefficient C_p, friction coefficient C_f and velocity distributions) are plotted in Figures 3–6. The WMLES results compare well with the DNS results, despite some minor deviation near the trailing edge as shown is Figure 4. The friction coefficient C_f varies from negative to positive near the trailing edge, indicative of a separation bubble on the suction side. The separation bubble is also observed in the contour plot

of the flow field as shown in Figure 6. The length of the separation bubble is much larger than that observed in the same case but $AoA = 0°$. The velocity distributions as shown in Figure 5 also indicate flow reverse in the separation zone. This favorable comparison between DNS and WMLES implies that the present wall model is capable of capturing the near-wall flow characteristics well.

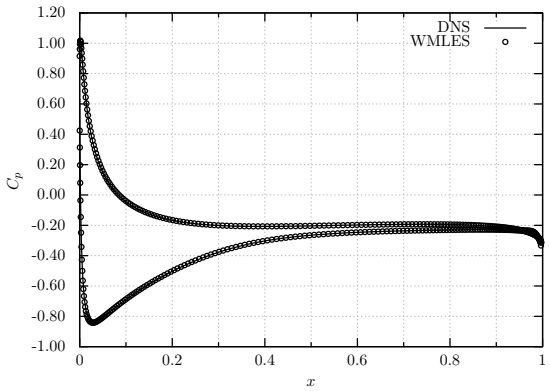

Figure 3: Distribution of the time- and spanwise-averaged pressure coefficient C_p around the airfoil (NACA0012, $AoA = 5°$, $Re = 10^4$).

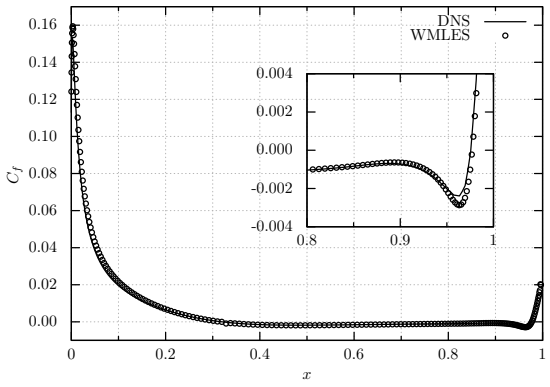

Figure 4: Distribution of the time- and spanwise-averaged friction coefficient C_f on the suction side (NACA0012, $AoA = 5°$, $Re = 10^4$).

NACA4412 Case: The time- and spanwise-averaged results for NACA4412 (pressure coefficient C_p, friction coefficient C_f and flow filed) are plotted in Figure 7–9. The WMLES results are compared with the DNS results from Hosseini *et al.* (2016) [13]. It should be noted that the domain size in the DNS is much smaller than that in the WMLES, especially the spanwise domain size in the DNS is just $0.1C$ compared with $0.8C$ in the WMLES case. The pressure coefficient C_p compares well the DNS results although some differences are found on the pressure side as shown in Figure 7. The comparison of friction coefficient is not as satisfactory. The C_f in the DNS results of Hosseini *et al.* (2016) show a very large excursion at about $x = 0.1C$: the WMLES C_f does not exhibit this feature. One may attribute this to lack of sufficient resolution near the leading edge in WMLES to capture this rapid variation in C_f. However, we can reproduce the same separation near the trailing-edge. We further note that the velocity contours as shown in Figure 9 are quite similar to that published in Hosseini *et al.* (2016) [13].

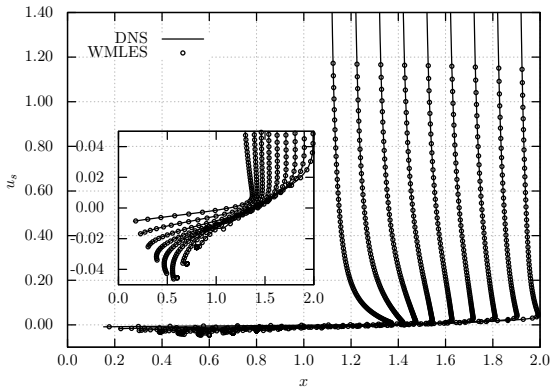

Figure 5: Streamwise velocity distribution along the suction surface from $x = 0.1$ to $x = 0.9$. The velocity profiles are artificially separated from each other by a displacement of 0.1 for clarity (NACA0012, $AoA = 5°$, $Re = 10^4$).

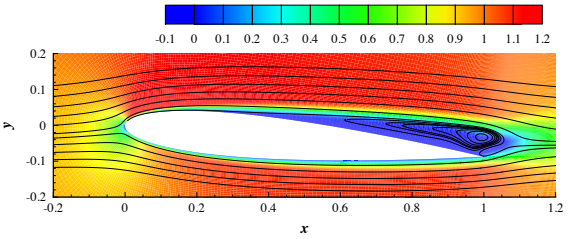

Figure 6: Streamlines superimposed with contours of the time- and spanwise-averaged x-component of the velocity field from WMLES (NACA0012, $AoA = 5°$, $Re = 10^4$).

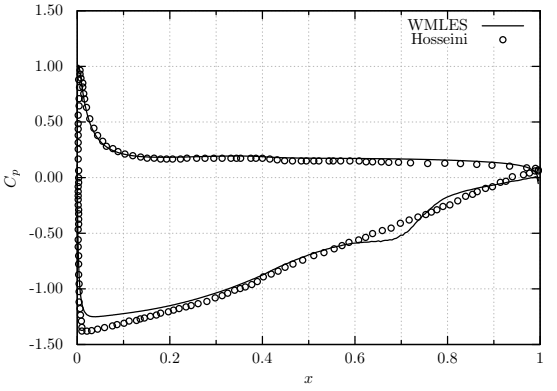

Figure 7: Distribution of the time- and spanwise-averaged pressure coefficient C_p around the airfoil (NACA4412, $AoA = 5°$, $Re = 4 \times 10^5$).

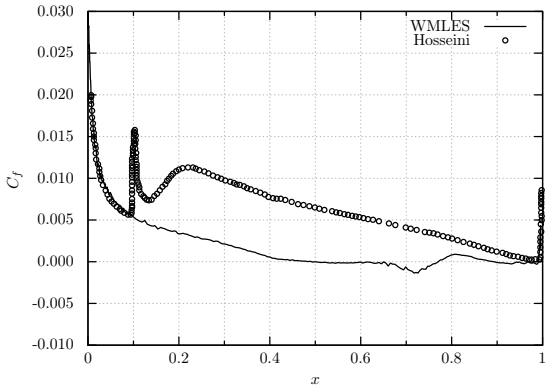

Figure 8: Distribution of the time- and spanwise-averaged friction coefficient C_f on the suction side (NACA4412, $AoA = 5^\circ$, $Re = 4 \times 10^5$).

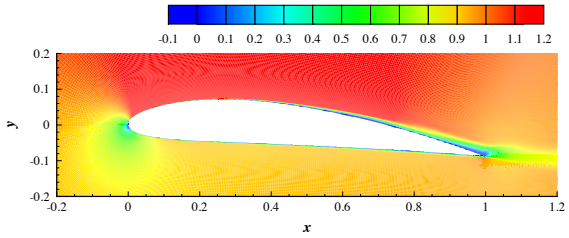

Figure 9: Contours of the time- and spanwise-averaged x-component of the velocity field from WMLES (NACA4412, $AoA = 5^\circ$, $Re = 4 \times 10^5$).

Conclusions

The virtual wall model is extended to the generalized curvilinear coordinates, which is coupled with the stretched-spiral vortex model to perform wall-modeled large-eddy simulations (WMLES) of turbulent flows over different airfoils. For the NACA0012 case with the lower Re, the WMLES results compare well with our DNS results, and the wall model is able to capture the separation bubble. For the NACA4412 case with high Re, the WMLES code behaves well in predicting the pressure coefficient. However the friction coefficient comparison with DNS results is not as favorable, and may be attributed to low resolution near the leading edge. Our future plan is to analyze the turbulent statistics and validate the WMLES code against experimentally data.

Acknowledgements

The work was supported by the KAUST office of Competitive Research Funds under Award No. URF/1/1394-01. The Shaheen-Cray XC40 at KAUST was utilized for all the simulations.

References

[1] Piomelli U., Wall-layer models for large-eddy simulations, *Prog. Aerosp. Sci.*, **44**, 2008, 437–446.

[2] Choi H. and Moin P., Grid-point requirements for large eddy simulation: Chapman's estimates revisited, *Phys. Fluids*, **24**, 2012, 011702.

[3] Park G. I. and Moin P., Numerical aspects and implementation of a two-layer zonal wall model for LES of compressible turbulent flows on unstructured meshes, *J. Comput. Phys.*, **305**, 2016, 589–603.

[4] Chung D. and Pullin D. I., Large-eddy simulation and wall modelling of turbulent channel flow, *J. Fluid Mech.*, **631**, 2009, 281–309.

[5] Inoue M. and Pullin D. I., Large-eddy simulation of the zero-pressure-gradient turbulent boundary layer up to $Re_\theta = O(10^{12})$, *J. Fluid Mech.*, **686**, 2011, 507–533.

[6] Saito N., Inoue M. and Pullin D. I., Large eddy simulation of smooth-wall, transitional and fully rough-wall channel flow, *Phys. Fluids*, **24**, 2012, 075103.

[7] Cheng W., Pullin D. I. and Samtaney R., Large-eddy simulation of separation and reattachment of a flat plate turbulent boundary layer, *J. Fluid Mech.*, **785**, 2015, 78–108.

[8] Misra A. and Pullin D. I., A vortex-based subgrid stress model for large-eddy simulation, *Phys. Fluids*, **9**, 1997, 2443–2454.

[9] Morinishi Y., Lund T. S., Vasilyev O. V. and Moin P., Fully conservative higher order finite difference schemes for incompressible flow, *J. Comput. Phys.*, **143**, 1998, 90–124.

[10] Zang Y., Street R. L. and Koseff J. R., A non-staggered grid, fractional step method for time-dependent incompressible Navier-Stokes equations in curvilinear coordinates, *J. Comput. Phys.*, **114**, 1994, 18–33.

[11] Zhang W., Cheng W., Gao W., Qamar A. and Samtaney R., Geometrical effects on the airfoil flow separation and transition, *Comput. Fluids*, **116**, 2015, 60–73.

[12] Zhang W. and Samtaney R., Assessment of spanwise domain size effect on the transitional flow past an airfoil, *Comput. Fluids*, **124**, 2016, 39–53.

[13] Hosseini S. M., Vinuesa R., Schlatter P., Hanifi A. and Henningson D. S., Direct numerical simulation of the flow around a wing section at moderate Reynolds number, *Int. J. Heat Fluid Flow*, 2016, in press.